

Notch Fatigue Property of 7050-T7451 Aluminum Alloy under Bending Resonance Environment

Dingni HE*, Wei CUI*, Yunfei LIAO**, Jianbo ZHANG**

*China Helicopter Research and Development Institute, Jingdezhen, 333001, China, E-mail: shine.1990.hi@163.com (Corresponding author)

**Shanghai Aeronautical Materials & Structures Testing Co., LTD, Shanghai, 200120, China

<https://doi.org/10.5755/j02.mech.33709>

1. Introduction

Helicopter components are subjected to environments with complex vibrations and cyclic loadings under flight conditions, and fatigue fracture accidents caused by localized resonance have occurred frequently in recent years. Fatigue analysis can be generally categorized into conventional fatigue analysis and resonant fatigue analysis. Resonant fatigue analysis is suitable for considering the resonant effect in cases in which the frequency of excitation loads includes the natural frequency of the system [1]. In this case, the resonant fatigue analysis of helicopter components becomes an interesting research hotspot in the scientific community [2-6].

Due to the needs of actual design, there will be some geometrically discontinuous such as notches existing in the structural components, which can serve as stress raisers and favorable zones for crack initiation, therefore reducing the fatigue strength of the components [7-11]. A lot of research has been devoted to study the effect of notches on the fatigue fractures under constant amplitude and variable amplitude loadings [12-16].

In the last decades, much attention has been focused on the metallic notch fatigue behavior under vibration environments in literature. Luo et al. [17-19] designed a novel testing equipment installed on a triaxial shaker table and implemented a vibration fatigue analysis of notched metallic structures subjected to multiaxial random vibrations. Prasad and Sekhar [20] compared the experimental fatigue life of a notched rotating shaft with an estimated life using traditional $S-N$ curve, time domain and spectral domain methods. Mohamed et al. [21] conducted experimental tests to examine the vibration characteristics in two different types of cracks in a long rotor shaft, a notch cut of varying depths and actual crack growth from a pre-crack. Torizuka et al. [22] carried out electromagnetic resonance fatigue testing on notched specimens at 150 Hz up to 10^7 cycles, and found that the notch fatigue limit increased with an increase of tensile strength. Li et al. [23] and Patil [24] predicted the vibration fatigue life of weld toe by notch stress approach. Chien et al. [25] and Yu et al. [26] conducted an investigation on the fillet rolling and resonant bending fatigue tests of crankshafts sections by finite element analyses and experiments. The fatigue property of notched components under vibration loadings has attracted the interests of researchers, but there are few studies on the fatigue property of notched specimens under resonant states. For the anti-resonance fatigue design of helicopter structures, there is still a lack of basic data on notch fatigue property under resonance environment.

The objective of this study is to obtain the notch fatigue property of 7050-T7451 aluminum alloy under bending resonance environment. For this objective, a resonant fatigue testing system and corresponding conventional fatigue testing system were devised. Also, a series of fatigue tests and analyses were carried out.

The framework of the present paper is described as follows. In Section 2, the experimental details (specimen design, resonant fatigue testing system and conventional fatigue testing system) are summarized. In Section 3, the experimental results of the resonant and conventional fatigue tests are displayed. In Section 4 and 5, the results obtained are discussed and some conclusions are drawn respectively.

2. Experimental details

2.1. Specimen design

Fatigue test is a basic method to obtain material fatigue property. Many fatigue testing methods have standard specifications such as ASTM, ISO, HB, industrial standards or other testing standards. In this paper, the smooth specimens shown in Fig. 1, a are designed according to the HB 5277-84 [27]. The geometric size of the notched specimens is shown in Fig. 1, b, a round hole with a diameter of 1 mm is used to simulate the notch in the center of the specimen. The specimens are made of 7050-T7451 aluminum alloy, a typical material used in aviation, with a Young's modulus of 72 GPa, a density of 2780 kg/m³, a yield strength of 393 MPa, an ultimate tension strength of 496 MPa and a Poisson's ratio of 0.27 according to the AMS 4050J. The chemical composition weight percentage of 7050-T7451 is shown in Table 1. The 5.5 mm diameter hole in the specimen is used to fix the counterweight and accelerometer under resonance environment and to apply loads in conventional fatigue test.

To provide a quantitative description for the stress concentration severity of the notched specimens, the concept of theoretical stress concentration factor K_t is defined by [28]:

$$K_t = \frac{\text{the maximum stress at notch tip, } \sigma_{max}}{\text{the nominal stress, } \sigma_n}. \quad (1)$$

The stress concentration factor is usually determined by three methods: test method, look-up table method and finite element method. With the development of finite

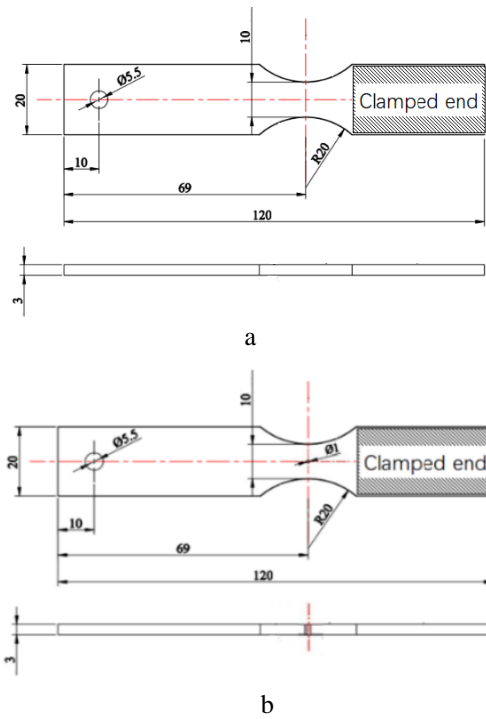


Fig. 1 Dimensions in mm: a - smooth specimen, b - notched specimen

Chemical composition

Element	min	max
Silicon	--	0.12
Iron	--	0.15
Copper	2.0	2.6
Manganese	--	0.10
Magnesium	1.9	2.6
Chromium	--	0.04
Zinc	5.7	6.7
Titanium	--	0.06
Zirconium	0.08	0.15
Other Elements, total	--	0.2
Aluminum	remainder	

element numerical analysis methods, the advantages of finite element method are more and more obvious, because it is applicable to various shapes of notches and boundary conditions, saving costs, so it is more and more widely used. A linear elastic numerical model of the notched specimen (Fig. 1, b) is simulated in ABAQUS. Fixed support constraints are applied at the clamped end, linear hexahedral elements are used to mesh the model with a total of 133584 elements and the maximum stress at notch tip is 75.0 MPa under a load of 10 N applied at the 5.5 mm diameter hole as is shown in Fig. 2. Fig. 3 shows the theoretical stress distribution of the notched specimen subjected to bending load. It can be known that the nominal stress is $6Fl/((W-d)r^2)$. When the external load $F = 10$ N, the nominal stress is 43.7 MPa. According to Eq. (1), the stress concentration factor is 1.72.

2.2. Resonant fatigue testing system

The resonant fatigue testing system used in this paper is composed of a Spider-80X vibration controller, an EDM-3200 electromagnetic shaker table, a VSA-H323A

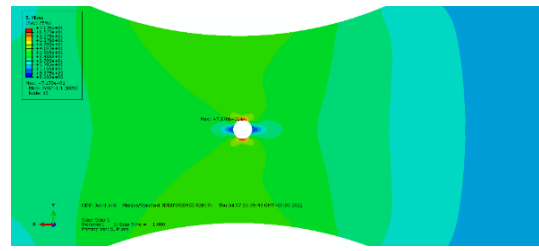


Fig. 2 The maximum stress at notch tip calculated by finite element analysis

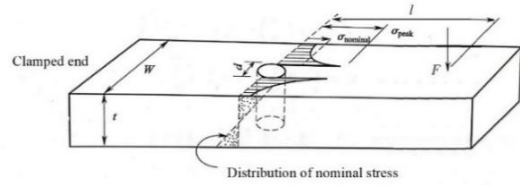


Fig. 3 The theoretical distribution of nominal stress on notched specimen

power amplifier, measurement and control system (a DH5921 dynamic signal testing analyzer, some 352C03 accelerometers, etc.), as shown in Fig. 4. The smooth and notched specimens are installed on the fixture with bolts, ensuring that the clamped end is fixed and restrained, and that the fixture is installed on the slip table (Fig. 5). The specimens are excited by an electromagnetic shaker table in the direction along their thickness.

The resonant fatigue test is to obtain the material properties under the premise of resonance of the specimen. Therefore, it is necessary to obtain the natural frequency of the specimen under the corresponding modal shape, and the resonance condition can be reached by using this natural frequency for test excitation. Based on the fundamental

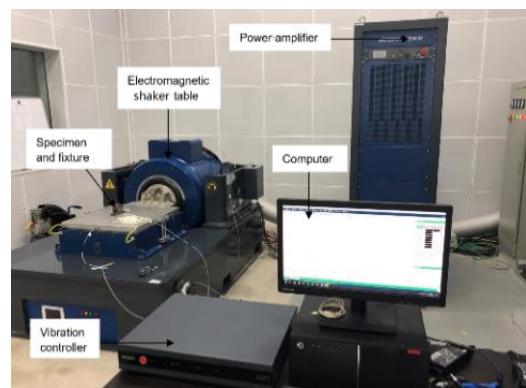
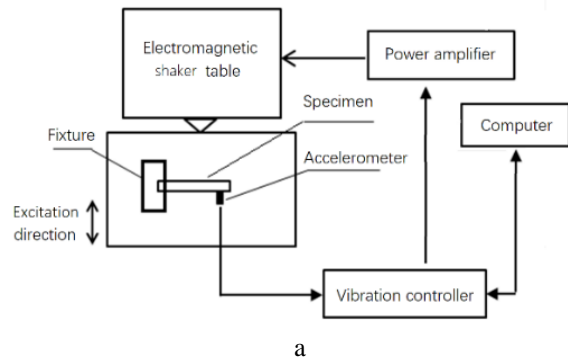


Fig. 4 Diagrams of the resonant fatigue testing system: a - schematic, b - physical

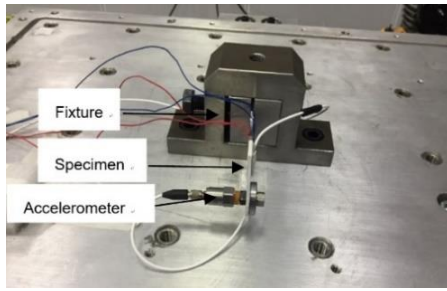


Fig. 5 Installation drawing of specimen and fixture

principle of modal analysis, the method of force-hammer excitation was adopted to conduct modal testing. The boundary condition of the specimen was consistent with that in Fig. 5, and displacement sensors were arranged at appropriate positions of the specimen. The displacement data of the measuring points were imported into the modal analysis and processing system software by force-hammer excitation method to extract the modal parameters. The results of model testing show that the first-order bending modal frequency is 124 Hz.

A strain gauge is attached to the minimum cross-sectional area of the specimen, and a counterweight sheet as well as a response accelerometer is arranged at the end of the specimen. Ensure the level state of the specimen during installation. Before the test, the relationship between response acceleration and strain was calibrated through base excitation. The response of calibration target started from 40 g, the difference in target response level was 10 g, and the calibration ended at 120 g. The mean value of strain collected at each level was converted into stress through formula $\sigma = E \cdot \varepsilon$, and finally the response acceleration-stress curve (calibration curve as shown in Fig. 6) was obtained.

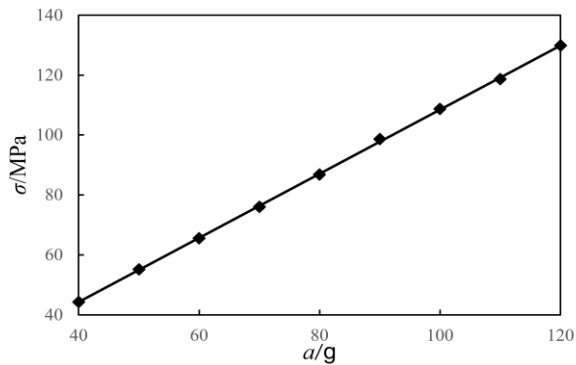


Fig. 6 Calibration curve of stress and response acceleration in working section of specimen

The stress on the dangerous section is characterized by response acceleration instead of strain value, through which the damage of strain gauge caused by the deformation of the dangerous section can be avoided and the reliability of data can be ensured. The initial excitation acceleration is determined according to the stress level of the dangerous point, which is kept unchanged during the test. In order to ensure that the specimen is always in the first-order resonance state, the resonance dwell method is adopted in the testing system, that is, the phase difference between the excitation acceleration and the response acceleration is guaranteed to be 90° by the control program. Stress ratio is -1 through this testing method. The parameters monitored during the resonant fatigue test are response acceleration

and frequency. Based on HB 5277-84 [27] and a large number of previous experimental studies, it has been found that when the natural frequency of specimen decreased by 2%, the specimen was close to the fracture state, cracks can be found by stereomicroscope, and obvious detectable cracks or fracture would occur rapidly after continued loading. Therefore, the stopping criterion of the resonant fatigue test is that the response acceleration drops sharply, the natural frequency drops by more than 2%, or the cycle number reaches 10^7 cycles.

2.3. Conventional fatigue testing system

In order to carry out a comparative analysis and research on the bending resonant fatigue and the corresponding conventional fatigue properties of the specimens, a conventional fatigue testing system is designed based on the resonant fatigue testing system, as shown in Fig. 7. A push rod is used in the system to connect the end of the specimens, which is of smooth and notched types respectively. The specimens are installed on a fixture (shown as Fig. 8), and the loads along the thickness direction of the specimens are applied by controlling the displacement of the electromagnetic shaker table.

A strain gauge is attached to the minimum cross-sectional area of the specimen, and a push rod as well as force sensor is arranged at the end of the specimen. During the installation, the level of the specimen is first guaranteed by a cushion block, and then the fixture and the clamped end of the specimen are tightened with bolts to ensure that the specimen is fixed constraint. After removing the cushion block, no additional bending moment will exist during the test. Before the test, the relationship between the input displacement peak value and strain value was calibrated based on the input displacement of the electromagnetic

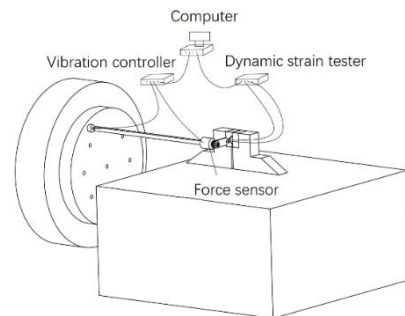


Fig. 7 Schematic diagram of the conventional fatigue testing system

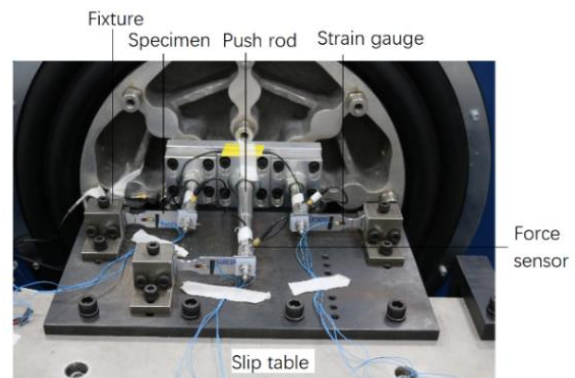


Fig. 8 Installation drawing of specimen and the fixture

shaker table, and the displacement peak value-stress curve (calibration curve as shown in Fig. 9) was obtained.

The input displacement peak is determined according to the stress level at the dangerous point, which is kept unchanged during the test, and the stress ratio is consistent with that of the vibration fatigue test ($R = -1$). The loading frequency is 20 Hz. The parameter monitored during the conventional fatigue tests is force. When cracks

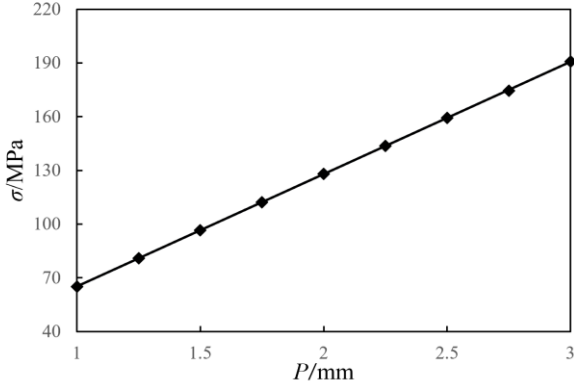


Fig. 9 Calibration curve of stress and displacement peak value in working section of specimen

occur in the dangerous section of the specimens, their response force drops sharply. Therefore, the sharp decline of response force of the specimens, the cracks of the specimens or the cycle number reaching 10^7 cycles are taken as the stopping criterion of the conventional fatigue tests.

3. Results

3.1. Resonant fatigue testing results

A total of 27 effective notched specimens were completed in the resonant fatigue tests, including 15 pieces at 3 stress levels through grouped method and 12 pieces through up-and-down method, and the test results are shown in Table 2. While a total of 23 effective smooth specimens were completed in the resonant fatigue tests, including 15 pieces at 3 stress levels through grouped method and 8 pieces through up-and-down method, and the test results are shown in Table 3. In the process of the bending resonant fatigue test, the excitation acceleration was always kept unchanged. According to the calibration relationship of $a - \sigma$ curve before the test, the excitation acceleration was converted to the initial danger zone stress, and the stress level of the specimens was characterized by the initial danger zone stress.

3.2. Conventional fatigue testing results

A total of 26 effective notched specimens were completed in the conventional fatigue tests, including 16 pieces at 3 stress levels through grouped method and 10 pieces through up-and-down method, and the test results are shown in Table 4. While a total of 23 effective smooth specimens were completed in the conventional fatigue tests, including 15 pieces at 3 stress levels through grouped

Table 2

Resonant fatigue testing results of notched specimens

Serial number	Initial danger zone stress (MPa)	Number of cycles	Serial number	Initial danger zone stress (MPa)	Number of cycles
1	160	152215	15	120	251363
2	160	150006	16	100	1421367
3	160	141796	17	95	1154394
4	160	97685	18	95	>10000000
5	160	140081	19	95	2814478
6	135	185519	20	90	>10000000
7	135	126819	21	90	>10000000
8	135	187781	22	85	823493
9	135	235524	23	80	9918150
10	135	231575	24	80	8674920
11	120	378015	25	80	>10000000
12	120	298196	26	75	>10000000
13	120	235940	27	75	>10000000
14	120	852350		-	

Table 3

Resonant fatigue testing results of smooth specimens

Serial number	Initial danger zone stress (MPa)	Number of cycles	Serial number	Initial danger zone stress (MPa)	Number of cycles
1	256	66643	13	204	249945
2	256	67700	14	204	296762
3	256	91290	15	204	344132
4	256	99757	16	139	4385000
5	256	79850	17	132	2289000
6	235	111634	18	132	5103000
7	235	168376	19	132	7644792
8	235	96839	20	132	>10000000
9	235	134851	21	125	>10000000
10	235	151162	22	125	>10000000
11	204	295360	23	125	>10000000
12	204	253663		-	

Conventional fatigue testing results of notched specimens

Serial number	Initial danger zone stress (MPa)	Number of cycles	Serial number	Initial danger zone stress (MPa)	Number of cycles
1	160	93424	14	120	463138
2	160	96424	15	120	314435
3	160	94624	16	120	388824
4	160	83051	17	85	5200441
5	160	140011	18	80	1604959
6	135	257968	19	80	2839615
7	135	182458	20	80	3775109
8	135	189949	21	80	>10000000
9	135	182458	22	80	7596661
10	135	269461	23	75	>10000000
11	120	508476	24	75	>10000000
12	120	568475	25	75	>10000000
13	120	833549	26	75	>10000000

Table 5

Conventional fatigue testing results of smooth specimens

Serial number	Initial danger zone stress (MPa)	Number of cycles	Serial number	Initial danger zone stress (MPa)	Number of cycles
1	254	49390	13	205	108959
2	254	60890	14	205	773765
3	254	84816	15	205	482406
4	254	87736	16	148	297754
5	254	98416	17	148	926898
6	233	76568	18	141	>10000000
7	233	79858	19	141	>10000000
8	233	84390	20	141	3252538
9	233	107990	21	141	3149836
10	233	129720	22	134	>10000000
11	205	412275	23	134	>10000000
12	205	128926		-	

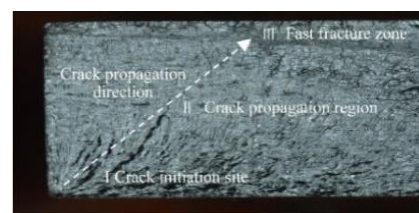
method and 8 pieces through up-and-down method, and the test results are shown in Table 5. During the bending conventional fatigue test, the peak of excitation displacement was kept unchanged. According to the calibration relation of $P - \sigma$ curve before the test, the peak of excitation displacement was converted to the initial danger zone stress. Consistent with the resonant fatigue test, the stress level of the specimens is characterized by the initial danger zone stress.

3.3. Fatigue fracture morphology

The specimen that has not yet completely broken (but has reached the failure criterion) in the test process was stretched along the vertical direction of the crack using an electronic universal testing machine, and the tensile process was based on the principle of not damaging the fracture surface. Then, ultrasonic cleaning was performed on all fractures, and the fracture morphology was observed under the stereomicroscope, as shown in Fig. 10. Although the fatigue crack growth history is different, the low magnification fracture morphology of the sample shows that it is mainly composed of three areas: fatigue crack initiation site, crack propagation region and fast fracture zone (the vibration fatigue specimen has not been tested to fracture, so the fast fracture zone is not obvious, as shown in Fig. 10, b).

Fig. 11 shows the SEM photos of the fatigue fracture morphology. The SEM analysis shows that there is transgranular fracture near the crack initiation site, a large

number of fatigue bands can be observed in the crack propagation region, there are diffusion prisms converging to the initial position of the crack in the fast fracture zone, the crack surface is relatively flat, and there are many parallel fatigue stripes on the crack surface. It can be seen that the fracture mechanism under bending resonant fatigue environment is roughly the same as that under bending conventional fatigue loading.



a



b

Fig. 10 Fracture morphology of specimens: a - conventional fatigue, b - vibration fatigue

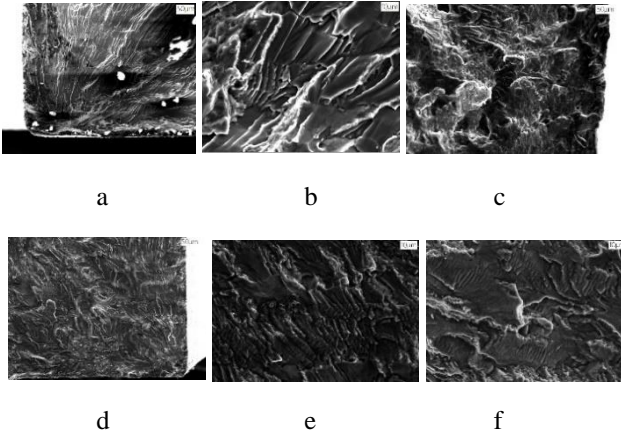


Fig. 11 Fracture morphology of conventional fatigue specimen under SEM: a - crack initiation site, b - crack propagation region, c - fast fracture zone and fracture morphology of resonant fatigue specimen under SEM: d - crack initiation site, e - crack propagation region, f - fast fracture zone

4. Discussion

4.1. $S-N$ curves

In the process of resonant and conventional fatigue tests, the maximum stress change in the dangerous zone of the specimens does not exceed 5%. The fatigue property of the material is described in this paper through the relationship between the initial danger zone stress S and the life N at the time of failure, that is, the $S-N$ curve. The expression of $S-N$ curve of the specimens is usually given by the power function fitting of three parameter [29]:

$$\lg N = a - b \times \lg(S_{max} - S_{\infty}), \quad (2)$$

where, a and b are material parameters, which varies according to the material and state of the specimen, S_{∞} is the corresponding material fatigue limit when the number of cycles is infinite, N is failure life, and S_{max} is the maximum stress, here is the initial danger zone stress. The test data of notched specimens and smooth specimens under resonant and conventional fatigue loading is fitted respectively, and the results in Table 6 are obtained. According to the data fitting results, the resonant and conventional fatigue $S-N$ curves of notched and smooth specimens of 7050-T7451 aluminum alloy are drawn, as shown in Fig. 12.

As can be seen from Fig. 12, in the range of 10^5 - 10^7 cycles, the $S-N$ curves of notched and smooth specimens of 7050-T7451 aluminum alloy show a continuously downward trend with the increase of cycle number, and there are no obvious horizontal progressive platforms or fatigue limits.

The stress amplitude corresponding to a certain cycle number is defined as the conditional fatigue limit for a continuous descending $S-N$ curve. At 1×10^7 cycles, the conditional fatigue limit of smooth specimens under resonant fatigue loading is 130 MPa, and that of notched specimens is 87 MPa. The conditional fatigue limit of smooth specimens under conventional fatigue loading is 141 MPa, and that of notched specimens is 78 MPa. Therefore, the notch fatigue property of 7050-T7451 aluminum alloy is far less than its smooth fatigue property under either

Table 6

Fitting results of $S-N$ curve parameters

Test items	$\lg N = a - b \times \lg(S_{max} - S_{\infty})$		
	a	b	S_{∞} (MPa)
Notch resonant fatigue test	7.512	1.279	84.155
Smooth resonant fatigue test	12.353	3.357	90.941
Notch conventional fatigue test	12.086	3.476	49.457
Smooth conventional fatigue test	12.435	3.506	105.534

resonance or conventional loading.

It can also be concluded from Fig. 12 that, for the resonant and conventional fatigue $S-N$ curves of smooth specimens, there exists a critical cycle of 3×10^5 within the cycle number range of 10^5 - 10^7 , and when $N < 3 \times 10^5$, the resonant fatigue life is longer than the conventional fatigue life; while when $N > 3 \times 10^5$, the resonant fatigue life is shorter than the conventional fatigue life. For the $S-N$ curves of the notched specimens, there are two critical cycles 2×10^5 and 3×10^6 , and when $N < 2 \times 10^5$ or $N > 3 \times 10^6$, the resonant fatigue life is longer than the conventional fatigue life; while when $2 \times 10^5 < N < 3 \times 10^6$, the resonant fatigue life is shorter than the conventional fatigue life.

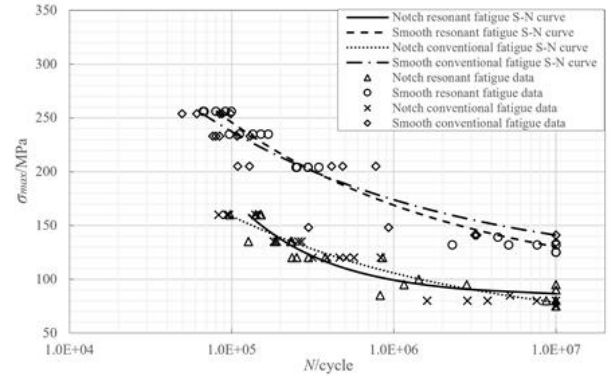


Fig. 12 Resonant fatigue and conventional fatigue $S-N$ curves of notched and smooth specimens of 7050-T7451 aluminum alloy

4.2. Notch sensitivity analysis

The fatigue notch factor K_f , plays a very important part in the estimation of fatigue life and fatigue property of structures in engineering. The most commonly accepted definition of K_f is the ratio of the fatigue limit of a smooth specimen σ_e to that of a notched specimen σ_N under the same experimental conditions with the same number of cycles [30]:

$$K_f = \frac{\text{fatigue limit of smooth specimen, } \sigma_e}{\text{fatigue limit of notched specimen, } \sigma_N}. \quad (3)$$

It has been widely observed and generally accepted that the fatigue notch factor is lower than the stress concentration factor K_t , and a notch sensitivity factor [31-32] can be described as

$$q = \frac{K_f - 1}{K_t - 1}, \quad (4)$$

in which the value of zero implies that the material is completely insensitive to the notch, and the factor of one implies that the material is fully notch-sensitive in that the fatigue notch factor equals to the stress concentration factor [33].

According to the parameter fitting results of $S-N$ curves shown in Table 6, the corresponding conditional fatigue limit, the fatigue notch factor K_f , and notch sensitivity factor q with a given failure cycle can be obtained.

Curves of fatigue notch factor (K_f) and notch sensitivity factor (q) with failure cycles are drawn in single logarithmic coordinates, as shown in Fig. 13. It can be seen that in the range of $10^5 - 10^7$ cycles, the notch fatigue property of 7050-T7451 aluminum alloy under bending resonance environment presents “stage characteristics”. There is a critical cycle number N_c of 8×10^5 , corresponding to the maximum fatigue notch factor K_{f-max} (or the maximum notch sensitivity factor q_{max}). When the cycle number of fatigue failure $N < N_c$, K_f increases with the increase of cycles, while when $N > N_c$, it decreases with the increase of cycles. It is shown that the notch sensitivity of 7050-T7451 aluminum alloy under resonant fatigue loading shows an increasing trend first and then decreases with the increase of cycles, that is, the notch fatigue property should be fully considered near the critical cycle number N_c . However, the notch fatigue property of 7050-T7451 aluminum alloy under conventional fatigue loading presents “linear characteristics”, that is, both K_f and q increase with the increase of cycles, which shows that with the increase of cycles, the notch sensitivity of 7050-T7451 aluminum alloy under conventional fatigue loading gradually increases. In practical engineering applications, the influence of stress concentration on the fatigue property of the material and the corresponding structure must be fully considered as the number of cycles increases.

When the conventional fatigue within 10^7 cycles, fatigue cracks initiate on the surface of the specimen, so the stress concentration on the surface of the specimen caused by the notch increases the surface plastic deformation, which promotes the formation of cracks. But when the failure cycle N is low, the stress amplitude S is high, the stress at the crack root exceeds the yield strength of the material, the notch root is passivated due to plastic deformation, so the stress concentration decreases, and the impact of notch stress concentration is low. With the increase of fatigue failure cycles N , the stress amplitude S decreases, and the influence of surface stress concentration will gradually increase. The fatigue notch factor K_f and notch sensitivity factor q increases with the increase of failure cycle N . That is, as shown in Fig. 13, the notch fatigue property of 7050-T7451 aluminum alloy under conventional fatigue loading presents “linear characteristics”. For resonant fatigue, the fatigue notch factor K_f and notch sensitivity factor q increase gradually when the failure cycle N increases from low to high, and its mechanism is similar to that of conventional fatigue. However, when the failure cycle N exceed a critical cycle number, the stress amplitude S further decreases. Under the resonance environment, the stress level at the notch of the dangerous section of the specimen is not prominent compared with the stress values at other positions of the dangerous section. Plastic deformation of specimen surface caused by notch stress concentration is not obvious, the influence of the surface stress concentration caused by the notch on the crack initiation will gradually weaken with the decrease of the stress amplitude S . Therefore, when the failure cycle N exceed a critical cycle number, the fatigue notch factor K_f

and notch sensitivity factor q decrease with the increase of failure cycle N , and the impact of notch stress concentration on fatigue property shows a downward trend. As shown in Fig. 13, the notch fatigue property of 7050-T7451 aluminum alloy under bending resonance environment presents “stage characteristics”.

For the conventional fatigue loading, the logarithmic value of N is linearly related to K_f and q in the range of $10^5 - 10^7$ cycles. For the resonant fatigue loading, the logarithmic value of N is linearly related to K_f and q in the range of $2 \times 10^6 - 1 \times 10^7$ cycles. These can be fitted as the following relations:

$$\begin{cases} K_f = K_0 - n \lg N \\ q = q_0 - m \lg N \end{cases}, \quad (5)$$

where, K_0 , q_0 , n and m are constants, which are related to the material and notch size of the specimens. Table 7 shows the fitting results of K_f and q with N in the two loading forms.

In the range of $10^5 - 10^7$ cycles, the notch fatigue property of 7050-T7451 aluminum alloy under resonant fatigue loading is different from that under conventional fatigue loading, that is, there are two critical cycles N_1 and N_2 . When $N < N_1$ or $N > N_2$, the notch fatigue property under conventional fatigue loading is larger than that under resonant fatigue loading. In this case, the influence of stress concentration on the conventional fatigue property of the material and corresponding structures must be fully considered. For structures where stress concentration is unavoidable in design, compared with resonance environment, fatigue performance will be reduced more in conventional environment. When $N_1 < N < N_2$, the notch fatigue property under resonance environment is larger than that under conven-

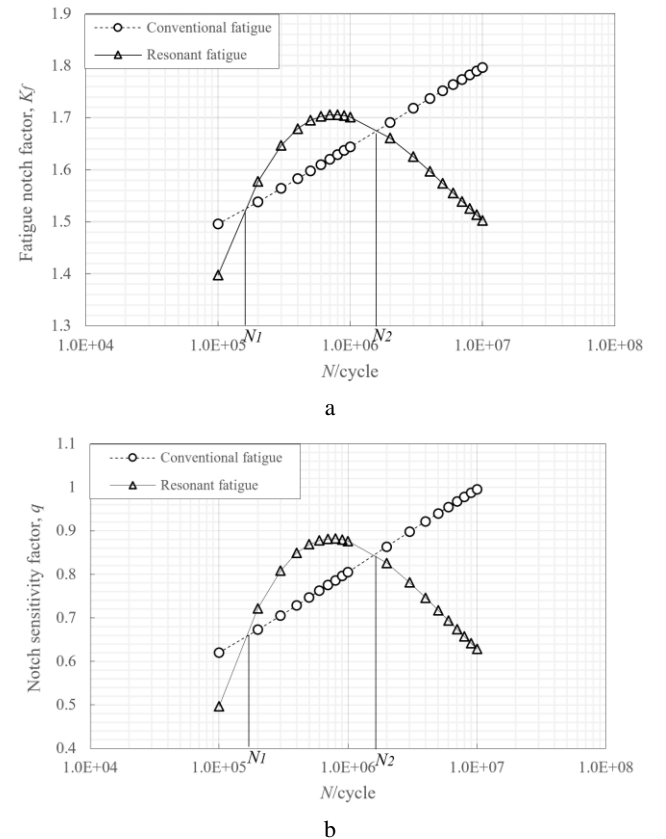


Fig. 13 The curves with failure cycles: a - fatigue notch factor, b - notch sensitivity factor

Table 7

 K_f and q curve parameters

Loading forms	K_0	n	q_0	m	Variance
Resonant fatigue	3.102	0.099	1.911	0.090	0.999
Conventional fatigue	0.732	0.066	0.244	0.060	0.999

tional fatigue loading, and the influence of stress concentration on the resonant fatigue property of the material as well as the corresponding structure must be fully considered. That is to say, the stress concentration is more sensitive under the resonance environment. Compared with the conventional fatigue environment, the design of stress concentration reduction under the resonance environment is required. For structures where stress concentration is unavoidable in design, resonance should be avoided as far as possible.

4. Conclusions

In this paper, both resonant and conventional fatigue tests on notched and smooth specimens of 7050-T7451 aluminum alloy have been carried out to investigate the notch fatigue property under bending resonance environment. The main conclusions are summarized as follows:

1. From the fracture surface of the specimen, it can be seen that the fracture mechanism under bending resonant fatigue environment is roughly the same as that under bending conventional fatigue loading.

2. The $S-N$ curves obtained through resonant fatigue tests show a continuously downward trend, and there are no obvious fatigue limits. The fatigue notch factor K_f equals to 1.49 at 10^7 cycles.

3. The $S-N$ curves obtained through conventional fatigue tests show a continuously downward trend, and there are also no obvious fatigue limits. The fatigue notch factor K_f equals to 1.81 at 10^7 cycles.

4. Notch fatigue property under bending resonance environment presents “stage characteristics”, which increases first and then decreases with the increase of cycles. There is a critical cycle number N_c at 8×10^5 cycles, corresponding to the maximum fatigue notch factor K_{f-max} (or the maximum notch sensitivity factor q_{max}).

5. Notch fatigue property under conventional fatigue loading presents “linear characteristics”, both K_f and q increase with the increase of cycles.

6. There are two critical cycles N_1 and N_2 . When $N_1 < N < N_2$, the notch fatigue property of the material and the corresponding structures under bending resonance environment requires more consideration than conventional fatigue loading.

Acknowledgements

The authors would like to acknowledge the support by the Civil Aircraft Pre-research Project of China (MJ-2017-F-21).

References

1. **Moon, S.I.; Cho, I.J.; Yoon, D.** 2011. Fatigue life evaluation of mechanical components using vibration fatigue analysis technique, *Journal of Mechanical Science and Technology* 25(3): 631-637.

- <http://doi.org/10.1007/s12206-011-0124-6>.
2. **Witek, L.; Wierzbinska, M.; Poznanska, A.** 2009. Fracture analysis of compressor blade of a helicopter engine, *Engineering Failure Analysis* 16(5): 1616-1622. <https://doi.org/10.1016/j.engfailanal.2008.10.022>.
3. **Kee, Y.J.; Kim, S.H.; Han, J.H.; Jung, J.K.** 2012. Resonant fatigue testing of full-scale composite helicopter rotor blades, 15th European Conference on Composite Materials, Venice, Italy.
4. **Bednarz, A.** 2019. Influence of the cyclic hardening model on the results of the numerical analysis of fatigue life on example of the compressor blade, *Journal of KONES* 26(2): 7-14. <https://doi.org/10.2478/kones-2019-0026>.
5. **Weiss, F.; Kessler, C.** 2021. Load prediction of hingeless helicopter rotors including drivetrain dynamics, *CEAS Aeronautical Journal* 12: 215-231. <http://doi.org/10.1007/s13272-020-00483-6>.
6. **Witek, L.** 2011. Crack propagation analysis of mechanically damaged compressor blades subjected to high cycle fatigue, *Engineering Failure Analysis* 18(4): 1223-1232. <https://doi.org/10.1016/j.engfailanal.2011.03.003>.
7. **Carter, T.J.** 2005. Common failures in gas turbine blades, *Engineering Failure Analysis* 12: 237-247. <https://doi.org/10.1016/j.engfailanal.2004.07.004>.
8. **Haritos, G.K.; Nicholas, T.; Lanning, D.B.** 1999. Notch size effects in HCF behavior of Ti-6Al-4V, *International Journal of Fatigue* 21: 643-652. [https://doi.org/10.1016/S0142-1123\(99\)00023-7](https://doi.org/10.1016/S0142-1123(99)00023-7).
9. **Banerjee, P.; Sarkar, R.; Pal, T.K.; Shome, M.** 2016. Effect of nugget size and notch geometry on the high cycle fatigue performance of resistance spot welded DP590 steel sheets, *Journal of Materials Processing Technology* 238: 226-243. <https://doi.org/10.1016/j.jmatprotec.2016.07.023>.
10. **Luo, P.; Yao, W.; Li, P.** 2019. A notch critical plane approach of multiaxial fatigue life prediction for metallic notched specimens, *Fatigue & Fracture of Engineering Materials & Structures* 42(4): 854-870. <https://doi.org/10.1111/ffe.12956>.
11. **Furnish, T.A.; Boyce, B.L.; Sharon, J.A.; O'Brien, C.J.; Clark, B.G.; Arrington, C.L.; Pillars, J.R.** 2016. Fatigue stress concentration and notch sensitivity in nanocrystalline metals, *Journal of Materials Research* 31(6): 740-752. <https://doi.org/10.1557/jmr.2016.66>.
12. **Fatemi, A.; Zeng, Z.; Plaseied, A.** 2004. Fatigue behavior and life predictions of notched specimens made of QT and forged microalloyed steels, *International Journal of Fatigue* 26(6): 663-672. <https://doi.org/10.1016/j.ijfatigue.2003.10.005>.
13. **Daemi, N.; Majzoob, G.H.** 2011. Experimental and theoretical investigation on notched specimens life under bending loading, *World Academy of Science, Engineering and Technology* 5: 2011-08-24.
14. **Bader, Q.H.; Njim, E.K.** 2014. Effect of V notch shape on fatigue life in steel beam made of AISI 1037, *International Journal of Engineering Research and Applications*, Vol. 4, Issue 6 (Version 6): 39-46.
15. **Susmel, L.; Taylor, D.** 2012. A critical distance/plane method to estimate finite life of notched components under variable amplitude uniaxial/multiaxial fatigue loading, *International Journal of Fatigue* 38: 7-24. <https://doi.org/10.1016/j.ijfatigue.2011.11.015>.

16. **Susmel, L.; Taylor, D.** 2013. The theory of critical distances to estimate finite life time of notched components subjected to constant and variable amplitude torsional loading, *Engineering Fracture Mechanics* 98: 64-79. <https://doi.org/10.1016/j.engfracmech.2012.12.007>.
17. **Luo, Z.; Chen, H.; He, X.** 2020. Influences of correlations between biaxial random vibrations on the fatigue lives of notched metallic specimens, *International Journal of Fatigue* 139: 105730. <https://doi.org/10.1016/j.ijfatigue.2020.105730>.
18. **Luo, Z.; Chen, H.; Zheng, R.; Zheng, W.** 2020. A damage gradient model for fatigue life prediction of notched metallic structures under multiaxial random vibrations, *Fatigue & Fracture of Engineering Materials & Structures* 43(9): 2101-2115. <https://doi.org/10.1111/ffe.13290>.
19. **Luo, Z.; Vantadori, S.; Ronchei, C.; Carpinteri, A.; Chen, H.** 2021. Vibration fatigue analysis of circumferentially notched specimens under coupled multiaxial random vibration environments, *Fatigue & Fracture of Engineering Materials & Structures* 44: 2412-2428. <https://doi.org/10.1111/ffe.13512>.
20. **Prasad, S.R.; Sekhar, A.S.** 2018. Life estimation of shafts using vibration based fatigue analysis, *Journal of Mechanical Science and Technology* 32(9): 4071-4078. <https://doi.org/10.1007/s12206-018-0806-4>.
21. **Mohamed, A.A.; Neilson, R.; Macconnell, P.; Renton, N.C.; Deans, W.** 2011. Monitoring of fatigue crack stages in a high carbon steel rotating shaft using vibration, *Procedia Engineering* 10: 130-135. <https://doi.org/10.1016/j.proeng.2011.04.024>.
22. **Torizuka, S.; Kuntz, M.; Furuya, Y.; Hoechst, M.B.** 2012. Effect of tensile strength and microstructure on notch-fatigue properties of ultrafine-grained steels, *ISIJ International* 52(5): 910-914. <https://doi.org/10.2355/isijinternational.52.910>.
23. **Li, F.; Wu, P.; Zeng, J.; Liu, C.; Wu, H.** 2019. Vibration fatigue dynamic stress simulation under multi-load input condition: Application to metro lifeguard, *Engineering Failure Analysis* 99: 141-152. <https://doi.org/10.1016/j.engfailanal.2019.02.024>.
24. **Patil, A.; Bhende, S.** 2021. Evaluation and validation of weld joint fatigue in vibration using notch stress approach, *Machine Mechanism and Robotics* 1169-1176. https://doi.org/10.1007/978-981-16-0550-5_111.
25. **Chien, W.Y.; Pan, J.; Close, D.; Ho, S.** 2005. Fatigue analysis of crankshaft sections under bending with consideration of residual stresses, *International Journal of Fatigue* 27(1): 1-19. <https://doi.org/10.1016/j.ijfatigue.2004.06.009>.
26. **Yu, V.; Chien, W.Y.; Choi, K.S.; Pan, J.; Close, D.** 2004. Testing and modeling of frequency drops in resonant bending fatigue tests of notched crankshaft sections, *Journal of Materials and Manufacturing, SAE Transactions* 113(5): 619-627. <https://www.jstor.org/stable/44699978>.
27. HB 5277-84. 1984. Vibration fatigue test method for engine blades and materials (in Chinese).
28. **Pilkey, W.D.; Pilkey, D.F.** 2008. *Peterson's Stress Concentration Factors*, 3rd ed, John Wiley and Sons, Inc., Hoboken.
29. **Yao, W.** 2019. *Fatigue life estimation of structures*, Beijing: Science Press 36 (in Chinese).
30. **Yao, W.; Xia, K.; Gu, Y.** 1995. On the fatigue notch factor, K_f , *International Journal of Fatigue*, 17, 4, 245-251. [https://doi.org/10.1016/0142-1123\(95\)93538-D](https://doi.org/10.1016/0142-1123(95)93538-D).
31. **Suresh, S.** 1998. *Fatigue of Materials*, 2nd ed, Cambridge University Press, New York.
32. **Dieter, G.E.** 1986. *Mechanical Metallurgy*, 3rd ed, McGraw-Hill, Boston.
33. **Furnish, T.A.; Boyce, B.L.; Sharon, J.A.; O'Brien, C.J.; Clark, B.G.; Arrington, C.; Pillars, J.R.** 2016. Fatigue stress concentration and notch sensitivity in nanocrystalline metals, *Journal of Materials Research* 31(6): 740-752. <https://doi.org/10.1557/jmr.2016.66>.

D. He, W. Cui, Y. Liao, J. Zhang

NOTCH FATIGUE PROPERTY OF 7050-T7451 ALUMINUM ALLOY UNDER BENDING RESONANCE ENVIRONMENT

S u m m a r y

Based on the electromagnetic shaker table, the resonant fatigue testing system and the corresponding conventional fatigue testing system were designed respectively. The fatigue life ($S-N$) curves of smooth and notched 7050-T7451 aluminum alloy specimens were measured in the range of $10^5 - 10^7$ cycles, and the notch fatigue property of 7050-T7451 aluminum alloy under bending resonance environment was studied. The results indicate that the fracture mechanism under bending resonant fatigue environment is roughly the same as that under bending conventional fatigue loading. All the $S-N$ curves obtained through resonant and conventional fatigue tests show a continuously downward trend, and there are no obvious fatigue limits. Notch fatigue property under bending resonance environment presents "stage characteristics", which increases first and then decreases with the increase of cycles. There is a critical cycle number N_c at 8×10^5 cycles, corresponding to the maximum fatigue notch factor K_{f-max} (or the maximum notch sensitivity factor q_{max}). There are two critical cycles N_1 and N_2 . When $N_1 < N < N_2$, the notch fatigue property of the material and the corresponding structures under resonance environment requires more consideration than conventional fatigue loading.

Keywords: notch fatigue property, bending resonance, conventional fatigue, 7050-T7451 aluminum alloy.

Received March 24, 2023

Accepted February 15, 2024



This article is an Open Access article distributed under the terms and conditions of the Creative Commons Attribution 4.0 (CC BY 4.0) License (<http://creativecommons.org/licenses/by/4.0/>).